A Chk1-Sp1-CD59 axis of the DNA damage response impedes rituximab-mediated complement-dependent cytotoxicity

Authors:
Allison S.Y. Chan[1], Patrick W. Jaynes[1], Akshaya Anbuselvan[1], Charmaine Z.Y. Ong[1], Michal M. Hoppe[2], Wai Khang Yong[1], Vartika Khanchandani[1], Jie Min Lee[1], Nurulhuda Mustafa[3], Muhamad Irfan Bin Azaman[1], Phuong M. Hoang[1], Guo Hong[4], Wee-Joo Chng[1,6,7], Mark S. Cragg[5], Dennis Kappei[1,8,9], Claudio Tripodo[10,11*], Anand D. Jeyasekharan[1,6-8*]

Affiliations:
[1]Cancer Science Institute of Singapore, National University of Singapore, Singapore, SG
[2]Singapore Translational Cancer Consortium, Consortium for Clinical Research and Innovation, Singapore, SG
[3]Department of Pharmacology, Yong Loo Lin School of Medicine, National University of Singapore, Singapore, SG
[4]Department of Laboratory Medicine, Southern University of Science and Technology Yantian Hospital, Shenzhen, CN
[5]Centre for Cancer Immunology, School of Cancer Sciences, University of Southampton, Southampton, UK
[6]Department of Haematology-Oncology, National University Cancer Institute- National University Health System, Singapore, SG
[7]Department of Medicine, Yong Loo Lin School of Medicine, National University of Singapore, Singapore, SG
[8]NUS Center for Cancer Research, Yong Loo Lin School of Medicine, National University of Singapore, Singapore, SG
[9]Department of Biochemistry, Yong Loo Lin School of Medicine, National University of Singapore, Singapore, SG
[10]Tumor Immunology Unit, Department of Health Sciences, University of Palermo, Palermo, IT
[11]IFOM ETS, The AIRC Institute of Molecular Oncology, Milan, IT
*Joint senior authors

To whom correspondence is to be addressed:
Anand D. Jeyasekharan
Cancer Science Institute of Singapore, National University of Singapore
#13-01G, 14 Medical Drive, Centre for Translational Medicine (MD6), Singapore 117599
Phone: +65-6516 5094, Email: csiadj@nus.edu.sg

Abstract

DNA damage responses primarily coordinate intracellular processes, but their effects on the cell surface remain poorly understood. We uncovered a DNA damage response at the cell surface that regulates complement dependent cytotoxicity (CDC), a key mechanism of antibody-mediated tumor cell killing. We found that several mCRPs, such as CD46, CD55, and CD59, are upregulated in diffuse large B-cell lymphoma (DLBCL) cells following chemotherapy. These mCRPs protect cells from CDC, including CDC triggered by anti-CD20 immunotherapy. Chemotherapy pre-treatment reduced the efficacy of rituximab-induced CDC, with CD59 exerting a dominant function. A high-throughput kinase screen revealed that Chk1 inhibition restored CDC sensitivity. Mechanistically, chemotherapy-induced CD59 expression was Chk1-dependent and regulated at an Sp1-driven promoter site. Inhibition of Sp1 with Mithramycin A abrogated chemotherapy-induced CD59 transcription. Co-immunoprecipitation mass spectrometry revealed that DNA damage releases transcriptional repressors from Sp1, an effect reversed by Chk1 inhibition. These findings define a Chk1-Sp1-CD59 signaling axis linking genotoxic stress to complement modulation. Our study reveals potential antagonism between chemotherapy and antibody-mediated CDC and highlights consideration in sequencing combination therapies and a therapeutic potential of Chk1 inhibitors in maintaining CDC efficacy during chemoimmunotherapy.

Short Summary: Rituximab-based chemoimmunotherapy is the first-line treatment for DLBCL. Our study reveals that chemotherapy induces resistance to rituximab-mediated cell killing. We identify this resistance as driven by a Chk1-Sp1-CD59 signaling axis and provide a therapeutic rationale for targeting this pathway to enhance chemoimmunotherapy efficacy.

Main Text

INTRODUCTION

The DNA damage response (DDR) is critical for maintaining genomic stability by coordinating cellular signaling events following genotoxic stress. While nuclear and cytoplasmic signaling pathways in the DDR are well-characterized, the extracellular signals triggered by DNA damage remain poorly understood. This gap limits our ability to optimize combination therapies that integrate genotoxic treatments with immunotherapies. A deeper understanding of DDR-mediated extracellular effects could illuminate how cancer cells interact with the immune microenvironment, offering new insights into therapeutic strategies for cancer [1].

Several cell surface proteins upregulated after DNA damage – such as MHC class I molecules, NKG2D ligands, CD95, and ICAM-1 – enhance tumor immunogenicity by increasing susceptibility to cytotoxic T cells and NK cells [2–4]. To further explore how the DDR influences cell surface changes, we previously employed a cell-surface phage display

screen using the isolation of antigen/antibody complexes through organic solvent (ICOS) method to characterize extracellular alterations triggered by the DDR [5,6]. This screen identified multiple phage particles preferentially binding to antigens on irradiated cell surfaces, including one to Ly6D [5]. Here, we investigate another target identified from the DDR-ICOS screen: a membrane-bound complement regulatory protein (mCRP).

Complement is a component of innate immunity and mediates cytotoxicity, leukocyte chemotaxis, and opsonization upon activation [7]. Host cells are protected from complement attack by expressing mCRPs, which include membrane cofactor protein (CD46), decay-accelerating factor (CD55), and protectin (CD59). CD46 and CD55 control C3/C5 convertase activation [8,9] while CD59 blocks the terminal complement pathway and subsequent lysis by preventing MAC formation [10]. Complement regulators are often overexpressed in different types of cancers, in line with the hypothesis that malignant cells adapt to avoid potential cell lytic MAC formation [11].

The complement system is activated by several therapeutic antibodies like rituximab, which can trigger complement-dependent cytotoxicity (CDC) upon binding the target antigen on malignant cells, as in the case of CD20 on B-cell lymphoma/leukemia cells [12]. Approved anti-CD20 monoclonal antibodies have various modes of cell killing, including direct killing (apoptotic and non-apoptotic), CDC, antibody-dependent cell-mediated cytotoxicity (ADCC), and antibody-dependent phagocytosis (ADP). As a type I-classified antibody, rituximab has a strong ability to activate complement and elicit CDC [13]. In diffuse large B-cell lymphoma (DLBCL), rituximab is a frontline therapy used in combination with chemotherapy. It is known that overexpression of mCRPs CD55 and CD59 inhibit rituximab-induced CDC, and blocking them enhances CDC efficacy [14,15]. This suggests the possibility of chemotherapy-induced mCRP upregulation in interfering with rituximab-induced CDC and potentially compromising treatment efficacy.

Here, we uncover a previously unrecognized mechanism by which DNA-damaging chemotherapy induces upregulation of mCRPs, potentially rendering tumor cells less responsive to antibody-based immunotherapy-induced CDC. To address this potential antagonism, we conducted a chemical screen and identified Chk1 inhibitors as agents capable of suppressing chemotherapy-induced mCRP expression while rescuing rituximab's cytotoxic activity. Sp1 is a known transcription factor that drives *CD59* expression [16]. Our investigation revealed that Chk1 regulates the association of Sp1 with transcription regulator Sp3 in a DNA damage-dependent manner. Our findings reveal a novel mechanism of resistance mediated by Chk1-mediated DNA damage response pathway and transcriptional control of mCRPs, with implications for improving regimens combining genotoxic agents and immunotherapeutic antibodies.

RESULTS

mCRPs CD46, CD55, and CD59 are upregulated upon chemotherapy treatment

To identify cell surface antigens upregulated post-DNA damage, we conducted a phage-display antibody (Ab) screen comparing X-ray irradiated cells and non-irradiated cells [5] (**Fig. 1A, Fig. S1A-C**). Using a published list of single-chain variable fragments (scFvs) that bound tumor-associated antigens as a frame of reference [17], we noted that several scFv sequences from our screen matched those previously identified as binding to membrane cofactor protein (MCP), also known as CD46. In a confirmatory experiment, X-ray irradiation of MCF10A cells displayed a dose-dependent increase of CD46 (**Fig. 1B**).

This finding led us to investigate more broadly mCRPs. Functionally, mCRPs (CD46, CD55, and CD59) prevent over-activation of the complement system. Studies have shown that mCRPs can interfere with anti-tumor treatments, especially antibody-induced CDC [18]. To investigate this, we modeled our study in cell lines from diffuse large B-cell lymphoma (DLBCL), an aggressive B-cell malignancy that is treated with an anti-CD20 monoclonal antibody, rituximab (RTX), generally used in combination with chemotherapy [19]. The DLBCL cell line SUDHL4 exhibited upregulated CD46 expression after treatment with various chemotherapy agents for 48 hours (**Fig. 1C**). The doses of chemotherapy used were chosen to evoke non-lethal DNA damage while maintaining approximately 80% cell viability (**Fig. S2A**). We chose etoposide as a genotoxic agent for subsequent experiments as a non-fluorescent topoisomerase inhibitor, compatible with flow cytometry assays. Using etoposide, we measured CD46, CD55, and CD59 levels in SUDHL4 cells (**Fig. 1D,1E**). CD46 and CD59 were significantly upregulated, while CD55 displayed moderate upregulation.

Chemotherapy abrogates rituximab-induced CDC via upregulation of CD59

The upregulation of mCRPs could impair the efficacy of rituximab treatment. Using an in-vitro CDC assay, we determined DLBCL cell line responsiveness to RTX-induced CDC (**Fig. S3A, 2A**). Sources of complement were normal human serum, and direct death could be ascertained using heat-inactivated serum. Within 2 hours, RTX induced effective cell death among various DLBCL cells via CDC and not via direct cytotoxicity, consistent with previous reports [13,20] (**Fig. 2A**). We observed that basal cell line sensitivity to rituximab-induced CDC was proportional to target CD20 expression (**Fig. 2B**). We pre-treated the CDC-sensitive SUDHL4 cell line with etoposide before performing the CDC assay and observed that RTX-induced CDC was impeded across its dynamic range (**Fig. 2C**). Using a RTX dose of 37 ng/mL, which is within the upper dynamic range, we confirmed that various genotoxic agents, such as those evoking replication-stress (gemcitabine, hydroxyurea) and DNA-damage (etoposide, doxorubicin) significantly impeded CDC (**Fig. 2D**). Interestingly, the microtubule-targeting agent vincristine did not impede CDC, further supporting a direct link between DNA damage induction and CDC impairment. As the sensitivity to rituximab-induced CDC is dependent on the expression of CD20, we assessed if the reduction of CDC efficacy in chemotherapy-treated cell lines was due to a downregulation of CD20. Using flow cytometry, we observed that cell surface levels of CD20 did not change upon treatment with etoposide (**Fig. 2E, 2F**). The lack of etoposide-induced CD20 downregulation confirms chemo-upregulated mCRPs as a specific phenomenon that correlated with the reduced CDC.

We then investigated the role of specific mCRPs in etoposide-abrogated CDC by using differentiating mCRP-neutralizing antibodies. Anti-CD55 (BRIC216) and anti-CD59 (YTH53.1) neutralizing antibodies were previously confirmed to block their targets at 10 µg/mL [21]. We ensured neutralization of CD46 with antibody CD46 (MC120.6) [22] by confirming it could bind to SUDHL4 cells (**Fig. S3B**) and that pre-incubation of the blocking antibody impeded the subsequent binding of the conjugated CD46-PE antibody in etoposide-treated cells (**Fig. S3C**). We tested the impact of each mCRP in the RTX-induced CDC response on etoposide-treated SUDHL4 cells by administering 10 µg/mL of mCRP neutralizing antibodies before the CDC assay (**Fig. 2G**). Anti-CD46 (MC120.6) and anti-CD55 (BRIC216) neutralizing antibodies did not rescue CDC, demonstrating levels comparable to etoposide-treated cells (**Fig. 2G**). In contrast, the anti-CD59 (YTH53.1) neutralizing antibody significantly rescued CDC, suggesting that CD59 is the key mCRP for mediating CDC resistance upon chemotherapy treatment.

Chk1 is a therapeutic target to recover rituximab-induced CDC efficacy

To identify targetable pathways that mediated the negative influence of chemotherapy on rituximab, we integrated a chemical drug screen with the CDC assay (**Fig. 3A**), we selected the Selleckchem kinase inhibitor library comprising 418 clinically tolerated compounds that can inhibit intracellular signaling pathways and are potent inhibitors of their targets in vivo (**Fig. 3B**). The library was applied at 1 µM concentration with or without etoposide treatment for 48 hours prior to the CDC assay (**Fig. 3A**). We then calculated and ranked the compounds based on the normalized cell viability of the etoposide condition compared to the control (**Fig. 3C**). Ranking hits allowed us to select compounds that enhanced cell death with CDC, and those below the 5th percentile of the screen (n=20 compounds) which were mostly enriched in compounds targeting DNA damage, especially Chk1 inhibitors, followed by ATM/ATR inhibitors (**Fig. 3D**). Validation of the ATR inhibitor VE-821 and Chk1 inhibitors Rabusertib, MK-8776, and CCT244747 (SRA737) showed that Chk1 inhibitors specifically recovered CDC sensitivity when administered alongside etoposide treatment (**Fig. 3E**). CDC rescue by Rabusertib was apparent in SUDHL4 cells and in another CDC-sensitive cell line, SUDHL6 (**Fig. 3F, 3G**). Notably, Rabusertib alone did not significantly increase CDC, suggesting that Chk1 is involved in DNA damage-induced abrogation of CDC.

Etoposide treatment activated Chk1, as indicated by the presence of phosphorylated Chk1 at Serine 345 (**Fig. 4A**). We thus hypothesized that activated Chk1 could be responsible for mediating the mCRP DNA damage response, and conversely, inhibiting Chk1 would block downstream signaling mediating this response. Indeed, combined treatment of etoposide and Rabusertib prevented the increase in mCRP in SUDHL4 cells (**Fig. 4B, 4C**) and other DLBCL cell lines (SUDHL6, SUDHL2, Karpas-231) (**Fig. 4D**). These results suggest that DNA damage induces Chk1-dependent regulation of mCRP levels.

Chk1 modulates transcription of mCRPs via release of Sp1-associated transcriptional repressors

Examining this phenomenon at the transcriptional level, we observed that transcripts of *CD46*, *CD55*, and *CD59* were upregulated in SUDHL4 cells after etoposide treatment, and that this upregulation was prevented by the addition of Rabusertib (**Fig. 5A, 5B, 5C**). This suggests that Chk1 regulates mCRP expression at the transcriptional level. We next examined potential transcriptional regulators downstream of Chk1 signaling, referencing a previous study by Du et al. that identified key transcription factors responsible for *CD59* expression (**Fig. 5D**) [16]. Briefly, Nf-κB and Sp1 control expression of Exon 1 (T1-4), while TP53 drives Exon 1' (T5) and CREB drives exon 1'' (T6-8). Our results show that etoposide primarily upregulates *CD59* expression at Exon 1 (T1-4), with no significant change in Exon 1' (T5) or Exon 1'' (T6-8) expression. Rabusertib consistently reversed expression at Exon 1 (T1-4) in SUDHL4 and SUDHL6 cells, suggesting that NF-κB or Sp1 could be primarily responsible for the altered expression (**Fig. 5E, Fig. S4A**).

It has been suggested that NF-κB may be primarily responsible for inducible expression of *CD59*, whereas Sp1 is responsible for constitutive expression [16]. Our experiments with NF-kB pathway inhibitors (QNZ, Dexamethasone, MLN120B, JSH-23) did not rescue CDC in the context of etoposide exposure (**Fig. S4B**). Strikingly, a specific inhibitor of Sp1, Mithramycin A [23], rescued CDC in SUDHL4 and SUDHL6 cells (**Fig. 5F, S4C**), as well as prevented the increase in CD59 expression (**Fig. 5G, 5H**). Consistent with this, Sp1 binding sites are present in all three mCRP promoters [24]. Additionally, Mithramycin A prevented the induced *CD46* expression (**Fig. S4D**). These results suggest that the observed upregulation of mCRPs occurs through DNA damage-induced Sp1 activity. Concordantly, treatment with Mithramycin A did not reduce basal mCRP expression, affirming that Sp1 primarily regulates the inducible expression of mCRPs (**Fig. S4E**). However, the DNA-damage induced increase in mCRP upregulation is unlikely due to an increase in total Sp1, since treatment with etoposide reduced total Sp1 levels (**Fig. 5I)**. We also observed that co-treatment of etoposide and Chk1i further reduced Sp1 levels and created a 70-kda Sp1 cleavage product, known to be caused by caspase activation [25] (**Fig. 5I**). This cleavage product was recognized by a polyclonal Sp1 antibody and CHIP-grade Sp1 (EPR22648) antibody which recognizes the C-terminus near the DNA binding domain, but was not recognized by another Sp1 antibody (E-3), which overlaps the caspase-cleavage site and ATM/ATR-phosphorylation site.

We therefore hypothesized that DNA damage could alter the Sp1-associated transcription complex. To investigate Sp1 protein interactions, we employed a co-immunoprecipitation label-free quantification mass spectrometry (Co-IP LFQ-MS) approach using the Sp1-specific antibody (EPR22548) in SUDHL4 cells (n=4 biological replicates). We compared three conditions: control (CTRL), etoposide treatment (ETO), and etoposide plus Rabusertib treatment (ETO+Chk1i) over 48 hours (**Fig. 6A**). We evaluated proteins that enriched within any of the conditions (respective Sp1 vs IgG) that met a significance cutoff of mean log2 fold enrichment (FE) and mean -log10 p-value > 2 (**Fig. 6B. 6C. 6D, S5A, Supplementary Tables 1-3**). Proteins enriched in any of the three conditions are displayed in a heatmap and organized by cellular compartment and function (**Fig. 6E, Fig. S5B**). Of the nuclear proteins, most of the Sp1-associated proteins were classified as transcription factors or epigenetic modulators (**Fig. 6E**). We focused on nuclear proteins with significant differential association

with Sp1 upon etoposide treatment and of which the association could be Chk1-dependent. Therefore, we selected proteins that had a |delta log2FE| > 2 between ETO and CTRL condition and whose levels reverted towards CTRL in the ETO+Chk1i condition (**Fig. 6F**). We identified a clear reduction of transcription factors NRF1, Sp3, ZNF740, and SPI1, and epigenetic factor RNF2 upon etoposide treatment. Conversely, we observed an increased association of Sp1 with HMBOX1 upon etoposide treatment. NRF1 is a context-dependent transcriptional regulator, while Sp3 and ZNF740 are known to be repressive [26–28]. SPI1 is a lineage-specifying transcription factor that regulates hematopoetic development, thus unlikely to have a universal role in mCRP expression, as we observed in MCF10A cells (**Fig. 1B**) [29]. Among epigenetic modulators, RNF2 is a component of the polycomb group (PcG) complex involved in gene repression and histone modification. HMBOX1 is a telomere-binding protein that regulates telomerase and is generally involved in negative regulation of transcription [30]. Of these candidate proteins, protein interactions between Sp1 and Sp3 have been previously confirmed by affinity chromatography and pull-down assays (**Fig. 6G**). We also interrogated Sp1 interactors which have been previously identified, including ZBTB5 and CDKN2A (**Fig. 6H**). Of interest is CDKN2A, which is only significantly associated with Sp1 upon treatment with etoposide and Chk1i. CDKN2A encodes the tumor suppressor ARF, which has been shown to inhibit Sp1-mediated transactivation or affect Sp1 protein stability [31]. Most candidate proteins suggest that Sp1 associates with transcriptional repressors, and dissociation upon etoposide treatment could explain a release in transcriptional repression. Overall, these results indicate that genotoxic stress disrupts Sp1 protein interactions with various repressive transcription factors (**Fig. 7**).

DISCUSSION

This study identifies a novel aspect of the DDR: the upregulation of mCRPs, which inhibit antibody-mediated CDC. Traditionally, cellular responses to DNA damage are viewed as cell-intrinsic processes such as cell cycle arrest, DNA repair, or apoptosis. However, emerging evidence—including our findings—suggests that DNA damage also triggers cell-extrinsic responses that modulate the surrounding microenvironment and influence immune responses. A well-known example is the upregulation of NKG2D ligands in response to DNA damage, which enhances recognition of stressed or damaged cells by natural killer cells and certain T cell subsets [4]. Our study demonstrates, for the first time, that cell-extrinsic mCRPs - specifically CD46, CD55, and CD59 - are also modulated in response to DNA damage, unveiling a regulatory mechanism triggered by DDR restraining cell/tissue damage and costimulation induced by complement cascade activation.

Using an ICOS screen, we identified mCRPs CD46, CD55, and CD59 as novel cell surface targets upregulated in response to DNA damage. In the context of DLBCL, we discovered that genotoxic agents antagonize rituximab's ability to trigger CDC. This antagonism was primarily attributed to the DNA damage-induced upregulation of CD59, though CD55 may also contribute in other cancer types [21,32].

To identify therapeutic strategies that could overcome this resistance, we performed a kinase library drug screen, which revealed Chk1 as a critical regulator of DDR-mediated mCRP expression. Inhibition of Chk1, when combined with etoposide treatment, effectively restored CDC activity by reducing the DNA damage-induced upregulation of CD59. These findings suggest that Chk1 inhibitors, in combination with chemotherapy, could be particularly beneficial when CDC plays a central role in tumor control.

We found that Mithramycin A rescued etoposide-induced mCRP expression by inhibiting Sp1-driven transcription [23]. Etoposide specifically increased inducible mCRP expression without affecting basal levels, indicating that Sp1 is a key driver of inducible mCRP expression. Notably, this transcriptional response was not linked to changes in Sp1 protein levels or cell cycle arrest. Instead, etoposide slightly reduced Sp1 levels, consistent with earlier studies showing Sp1 degradation through the ATM pathway following DNA damage [33].

An alternative explanation for our observations could lie in the interactions of other transcription factors with Sp1- a protein known to communicate with the RNA polymerase II transcription machinery, affect chromatin state, and interact with epigenetic regulators [34]. Co-immunoprecipitation mass spectrometry of Sp1-bound proteins revealed that Sp1 exhibits differential association with several transcriptional repressors and chromatin remodelers upon DNA damage, including Sp3, NRF1, ZNF740, and RNF2. Of particular interest is Sp3, known to repress Sp1-mediated transactivation of promoters with multiple Sp1-binding sites [26]. Notably, all mCRPs have multiple Sp1 sites (CD46, CD55 (3 sites), CD59 (2 sites)) [24], suggesting that the modulation of Sp1 activity could be influenced by its ratio with the repressive Sp3 transcription factor [35]. The observed abolishment of Sp3 interaction with Sp1 in the etoposide-treated condition suggests that competition for Sp1 binding at basal levels may regulate Sp1 promoter sites, potentially partially regulated by Chk1. Another possible mode of Chk1 inhibitor control of Sp1 levels is caspase cleavage. We observed that co-treatment with etoposide and a Chk1 inhibitor induced caspase cleavage of Sp1, producing an inactive 70 kDa fragment [8].

The potential of Chk1 inhibitors in cancer therapy has been explored in recent clinical trials [36]. Recently, CCT245737 (SRA737) displayed good tolerance and a favorable pharmacokinetic profile in a recent Phase I/II clinical trial (NCT02797964) [37]. While single-agent potency has been limited, combinations with chemotherapy agents have shown promise, such as low dose gemcitabine (NCT02797977) [38]. Studies of Chk1 inhibitors with chemotherapy agents (e.g., etoposide, gemcitabine) have also confirmed strong synergistic anticancer effects in cancer cell line models [39,40]. In our hands, SRA737 was able to effectively recover and enhance rituximab-induced CDC after etoposide treatment. We propose that the combination of emerging Chk1 inhibitors, such as SRA737, with chemotherapy not only demonstrates strong anti-cancer effects but also, in light of our findings on enhanced CDC, provides additional support for its potential to augment apoptosis and CDC-mediated anti-tumor responses.

The implications of our findings extend beyond complement-mediated lysis in tumors, impacting the broader immune contexture. The upregulation of mCRPs in response to DNA damage could confer a survival advantage to cancer cells by suppressing complement-mediated lysis and influencing immune evasion mechanisms. This may contribute to selection of tumor cells that emerge towards a more immune-evasive tumor population. In normal physiology, the upregulation of mCRPs in response to DNA damage may serve as a protective mechanism. In tissues undergoing stress or damage, this response could help prevent excessive complement-mediated lysis of cells, allowing time for DNA repair processes to occur. This mechanism might be particularly important in tissues frequently exposed to environmental stressors, such as the skin, kidney, or the gastrointestinal epithelium [41–43].

Within the context of therapy, our findings also have implications for therapeutic modalities involving T-cell engagers or CAR-T therapies, which can be impacted by complement. Anaphylatoxins c3a and c5a contribute to acute inflammation by activating various immune cells [11]. However, in many cancer types, these anaphylatoxins paradoxically increase recruitment of immunosuppressive cells and decrease the number of pro-inflammatory cells [11]. CD55, as a negative regulator of c3 and c5 convertases, inhibits anaphylatoxin production, suggesting a role for CD55 in contributing to an inflammatory tumor milieu. Additionally, CD46 is necessary for T cell function, activation, and IFN-γ generation [44]. Thus, in the context of cell-mediated therapy and depending on cancer type, the DDR-mCRP upregulation could potentially benefit therapeutic modalities involving T-cell engagers or CAR-T therapy, an avenue that remains to be further explored [45]. In such scenarios, we would likely avoid using Chk1 inhibitors or Mithramycin A to allow increased expression of mCRPs. Future translational studies in immune-competent models are required to determine the potential to improve antibody- and cell-based therapies immunotherapies.

In summary, our study identifies the Chk1-Sp1 axis as a novel mechanism by which DNA damage-induced mCRP upregulation mediates resistance to CDC, warranting careful consideration when combining DNA-damaging therapies with antibody-based immunotherapies. Indeed, incomplete activation of the classical complement cascade through DDR-induced mCRP upregulation could favor non-canonical role of complement in the tumor microenvironment, eventually favoring tumor progression [46]. Combining Chk1 inhibitors, Mithramycin A, or CD59-neutralizing antibodies with chemotherapy could enhance the efficacy of antibody-based therapies by subverting mCRP-mediated resistance. Additionally, our findings support use of genotoxins alongside cell-mediated therapy and bispecific antibodies, such as those which dually target CD59 and CD20 [47].

MATERIALS AND METHODS

Cell culture and reagents

MCF10A cells were cultivated in DMEM/F-12 (Dulbecco's Modified Eagle Medium/Nutrient Mixture F-12) medium (Invitrogen) containing 5% horse serum, 10 μg/ml insulin, 20 ng/ml

EGF, 100 ng/ml choleratoxin, 500 ng/ml hydrocortisone and 1% pen/strep and grown at 37 °C and 5% CO_2. Human DLBCL cell lines (DOHH2, HT, Karpas-231, Karpas-422, OCI-LY8, SC-1, SUDHL2, SUDHL4, SUDHL6, U2932) were cultured in RPMI-1640 (Roswell Park Memorial Institute 1640) medium supplemented with 20% heat-inactivated fetal bovine serum (FBS, HyClone Research Grade Fetal Bovine Serum, South American Origin) and grown at 37 °C and 5% CO_2. MCF10A, DOHH2, HT, SUDHL4, and SUDHL6 cell lines were authenticated with STR profiling by ATCC Cell Authentication. Cells were confirmed mycoplasma-free by MycoAlert® Mycoplasma Detection Kit (Lonza).

To maintain surface antigens prior to screening, MCF10A cells were harvested using enzyme-free cell dissociation buffer (Millipore), or StemPro Accutase Cell Dissociation Reagent (Invitrogen). Irradiation was performed at 3mA/130v on a Faxitron Cabinet X-Ray generator, with duration of exposure adjusted to define dosage. Compounds used are listed in Materials. For all drug treatment experiments, cells were plated at a ratio of 10^6 cells per 5mL media and treated with compounds for 48 hours. For Mithramycin A, cells were treated for 16 hours prior to collection due to cytotoxicity.

Cell lysis and immunoblotting

Cells were lysed in RIPA buffer (Thermo Scientific) containing 0.2mM MgCl2, 0.01U/]µL Benzonase® Nuclease (Merck Millipore), 1X protease inhibitor (Sigma), 1X phosphatase inhibitor (Sigma). Protein concentrations were determined by BCA assay (Thermo Scientific) and equal concentrations were diluted into NuPage™ LDS Sample Buffer and DTT. After electrophoresis, proteins were transblotted to PVDF membranes (Thermo Scientific). Blots were blocked with 5% skim milk/ TBS-Tween followed by incubation with primary antibodies overnight at 4°C. The blots were incubated with secondary antibodies conjugated with horseradish peroxidase (Cell Signaling Technology) and were then developed using Immobilon HRP substrate (Merck Millipore). Blots were visualized using a ChemiDoc Imaging System (Bio-rad). Antibodies used are listed in Materials.

Chemical screening

Chemical screening was performed at the Center for High-throughput Phenomics, Genome Institute of Singapore. Compounds were printed at 1µM on a 384-well tissue culture plate (Corning) with an acoustic liquid handler (Echo, Beckman Coulter Life Sciences). SUDHL4 cells were seeded at 10,000 cells/well in 25µL of RPMI-1640 + 20% heat inactivated FBS using the Biotek MultiFloFX Dispenser. Plates were sealed with Breathe-easy membrane (Sigma-Aldrich) and incubated at 37 °C and 5% CO_2 for 48 hours. 0.2 µg/mL rituximab was added using Echo, and plates were incubated for 30 minutes. 20% human serum (f.v.) was added using the Biotek MultiFloFX dispenser. After two hours of incubation, cell viability was measured using Cell Titer Glo (Promega) on a microplate reader (Tecan). The readout was normalized among duplicate replicates.

Co-immunoprecipitation and mass spectrometry

To isolate the nuclear fraction, cells were resuspended in buffer A (10mM HEPES-NaOH pH 7.9, 10mM KCl, 1.5mM MgCl2, 0.34M sucrose, 10% glycerol, 0.5mM DTT) plus protease inhibitor and phosphatase inhibitor tablets for 10 minutes on ice at 4°C and centrifuged (1300xg, 5 minutes). The nuclear pellets were then resuspended with Buffer B (3mM EDTA, 0.2mM EGTA, 1mM DTT, 0.3U/µL Benzonase) plus protease inhibitor and phosphatase inhibitor tablets for 30 minutes on ice at 4°C. 400µg of protein, determined by the BCA Protein Assay Kit (Thermo Scientific), was incubated with Sp1 antibody (EPR22648) or Rabbit Isotype IgG Control (Invitrogen) in IP Lysis buffer (10mM Tris pH 7.4, 150mM NaCl, 0.5mM EDTA pH 8, 0.5% NP-40, 0.25% sodium deoxycholate, 2mM MgCl2) plus protease inhibitor and phosphatase inhibitor tablets, overnight at 4°C on a rotating wheel. The lysate was then incubated with Dynabeads™ Protein A (Invitrogen) for 3 hours at 4°C on a rotating wheel, washed 4 times with IP buffer (10mM Tris pH 7.4, 150mM NaCl, 0.5mM EDTA pH 8, 0.5% NP-40, 0.25% sodium deoxycholate), and eluted with 2x Laemmli and beta-mercaptoethanol elution buffer by heating to 95°C for 5 minutes. Sp1 IP samples were analysed by label-free quantification mass spectrometry essentially as described in [18].

To this end, eluted proteins were separated by SDS-PAGE gel electrophoresis using NuPAGE 12 % Bis-Tris Mini Protein gels (Thermo Scientific) at 170 V for 10 minutes. Each sample was treated as a single fraction for in-gel trypsin digestion. Briefly, gel fractions were cut approximately into 2 by 2 by 1 mm pieces, destained twice using 1 ml Destaining Solution (50 % (v/v) ethanol, 25 mM ammonium bicarbonate) and dehydrated with 150 ul acetonitrile. Gel pieces were dried using a speed vacuum concentrator (Eppendorf) and subsequently treated with 200 ul Reducing Solution (10 mM DTT, 50 mM ammonium bicarbonate) at 56 °C for 1 hour followed by 200 ul Alkylating Solution (55 mM iodoacetamide, 50 mM ammonium bicarbonate) at room temperature for 45 minutes in the dark. Gel pieces were washed once with 200 ul 50 mM ammonium bicarbonate and twice with 150 ul acetonitrile, dried using a speed vacuum concentrator, and incubated with 2 µg sequencing grade trypsin (Promega) in 200 ul 50 mM ammonium bicarbonate at 37 °C overnight. Digested peptides were extracted from the gel pieces on the following day through two incubations each using an alternating cycle of 200 ul Extraction Buffer (3 % (v/v) trifluoroacetic acid, 30 % (v/v) acetonitrile, 33.3 % (v/v) mM ammonium bicarbonate) and 150 ul acetonitrile for 20 minutes and 10 minutes, respectively, followed by a final incubation in 150 ul acetonitrile for 10 minutes. All supernatants were collected and combined. Extracted peptides in solution were concentrated using a speed vacuum concentrator for 2 hours and desalted with home-made stage-tips containing C-18 resins (Empore). Stage tips were stored at 4°C prior elution of peptides with 30 ul Solution B (80 % (v/v) acetonitrile, 0.1 % (v/v) formic acid) for analysis using an EASY-nLC 1200 Liquid Chromatograph (Thermo Scientific) coupled to a Q Exactive HF (Thermo Scientific) mass spectrometer.

Peptides were separated on a C-18-reversed phase column (25 cm length, 75 µm inner diameter; New Objective) which was packed in-house with ReproSil-Pur 120 C18-AQ 1.9 µm resin (Dr Maisch). The column was mounted on an Easy Flex Nano Source and maintained at 40 °C by a column oven (Sonation). An 88-minute gradient from 2 to 40 % Solution B at a flow of 225 nl/minute was used, followed by a 12 minute washout with 95 %

Solution B. The spray voltage was set to 2.2 kV. The Q Exactive HF was operated with a TOP20 MS/MS spectra acquisition method per MS full scan, conducted with 60,000 at a maximum injected time of 20 ms and MS/MS scans with 15,000 resolution at a maximum injection time of 75 ms.

Raw files were processed with MaxQuant [48] version 2.0.1.0 with preset standard settings for label-free quantitation using at least 2 LFQ ratio counts based on the MaxLFQ algorithm [49]. Carbamidomethylation was set as fixed modification while methionine oxidation, protein N-acetylation, and serine, threonine and lysine (STY) phosphorylation were considered as variable modifications. Searches were performed against the human (UP000005640) Uniprot databases. Search results were filtered with a false discovery rate of 0.01. Known contaminants, proteins groups only identified by site, and reverse hits of the MaxQuant results were removed, and only protein entries with at least three of four non-zero values in either condition of each pair-wise comparison were included in the analyses. Missing LFQ intensity values were imputed three times using a random distribution centered around the lowest 5% of LFQ intensities, with the final values representing the mean of these three iterations.

Complement Dependent Cytotoxicity assay

Cells were incubated with rituximab (RTX) for 30 minutes in a 96-well solid white flat bottom plate (Corning) at a cell density of $2*10^5$ cells/mL. SUDHL4 cells were treated with 37ng/mL RTX, while SUDHL6 cells were treated with 12.5 ng/mL RTX unless indicated. Subsequently, human serum or heat-inactivated (complement-inactivating) serum was added to 10% v/v concentration and incubated for 2 hours. Cell viability was determined by Cell Titer Glo (Promega) with SparkControl V2.3 Tecan Microplate Reader at 1s integration. CDC was calculated using the following formula:

$$\%\, direct\, death = 100 * \left(1 - (R + HiHS/HS)\right)$$

$$\%\, CDC = 100 * \left(1 - (R + HS/HS)\right) - \%\, direct\, death$$

"R" represents rituximab, "HS" represents human complement serum, and "HiHS" represents heat inactivated human complement serum.

For mCRP neutralizing experiments, CD46 blocking antibody derived from the MC120.6 CD46 hybridoma (SFR Biosciences), CD55 antibody (BRI216) (Bio-Rad), or CD59 (YTH53.1) (Bio-rad) were added at 10µg/mL final concentration for 1 hour prior to the assay.

Flow cytometry

Flow cytometry was performed using the BD ® LSR II Flow Cytometer. Debris was excluded by gating out low FCS-A and SSC-A cells. Single cell populations were obtained by gating out FCS-H-low cells in a FCS-H v FSC-A plot. Cells were analyzed with FlowJo™ v10.8 Software (BD Life Sciences). Mean fluorescence intensity (MFI) was calculated using the median for unimodal cell populations. Integrated mean fluorescence intensity (iMFI) was

calculated for bimodal populations [50]. Relative MFI was calculated by normalizing each marker to the respective IgG control, then comparing the treatment to control condition [51].

RNA extraction and quantitative real-time PCR

Total RNA was extracted using RNeasy Mini kit (Qiagen) according to manufacturer's instructions and was reverse-transcribed to cDNA using iScript cDNA synthesis kit (BioRad). Quantitative real-time PCR was performed with PrecisionFAST qPCR Master Mix (Primerdesign Ltd) and primers (IDT, listed in Materials) on the Comparative-CT program on a QuantStudio 3 and 5 Real-Time PCR system (Fisher Scientific). Endogenous 18S was regarded as an internal control.

Statistical analysis

Statistical analyses and graphing were performed using GraphPad Prism 10.1.1 software (Graphpad, San Diego, CA, USA). For comparisons of two groups, statistical analysis was performed using paired t-tests, while ANOVA followed by post hoc Dunnet's multiple comparisons test to etoposide condition was used for multiple groups. Error bars represent SD of biological replicates. Statistical significance was denoted as follows (*) $p < 0.05$, (**) $p < 0.01$, (***) $p < 0.001$.

Acknowledgments

Donut charts and heatmaps were generated using Rstudio (V4.4.0). [52] Visuals were created with Biorender.com.

Supplementary Materials and Figures

Materials

Fig. S1 Phage-display Antibody Screen Design

Fig. S2 Chemotherapy Cell Viability

Fig. S3 MC120.6 CD46 Blocking Antibody Validation

Fig. S4 Etoposide-induced CD59 gene expression is rescued with Mithramycin A

Fig. S5 Etoposide treatment induces Chk1-dependent changes to the Sp1 interactome

Table S1 Co-immunoprecipitated proteins pulled down with SP1 vs IgG antibodies, identified by mass spectrometry within CTRL condition.

Table S2 Co-immunoprecipitated proteins pulled down with SP1 vs IgG antibodies, identified by mass spectrometry within ETO condition.

Table S3 Co-immunoprecipitated proteins pulled down with SP1 vs IgG antibodies, identified by mass spectrometry within ETO+Chk1i condition.

References:

1 Liu B, Zhou H, Tan L, Siu KTH, Guan X-Y. Exploring treatment options in cancer: Tumor treatment strategies. *Signal Transduct Target Ther* 2024; **9**: 175.

2 Sato H, Niimi A, Yasuhara T, Permata TBM, Hagiwara Y, Isono M *et al.* DNA double-strand break repair pathway regulates PD-L1 expression in cancer cells. *Nat Commun* 2017; **8**: 1751.

3 Uchihara Y, Permata TBM, Sato H, Kawabata-Iwakawa R, Katada S, Gu W *et al.* DNA damage promotes HLA class I presentation by stimulating a pioneer round of translation-associated antigen production. *Mol Cell* 2022; **82**: 2557-2570.e7.

4 Gasser S, Orsulic S, Brown EJ, Raulet DH. The DNA damage pathway regulates innate immune system ligands of the NKG2D receptor. *Nature* 2005; **436**: 1186–1190.

5 Kurosawa M, Jeyasekharan AD, Surmann E-M, Hashimoto N, Venkatraman V, Kurosawa G *et al.* Expression of LY6D is induced at the surface of MCF10A cells by X-ray irradiation. *FEBS J* 2012; **279**: 4479–4491.

6 Akahori Y, Kurosawa G, Sumitomo M, Morita M, Muramatsu C, Eguchi K *et al.* Isolation of antigen/antibody complexes through organic solvent (ICOS) method. *Biochem Biophys Res Commun* 2009; **378**: 832–835.

7 Walport MJ. Complement. First of two parts. *N Engl J Med* 2001; **344**: 1058–1066.

8 Kojima A, Iwata K, Seya T, Matsumoto M, Ariga H, Atkinson JP *et al.* Membrane cofactor protein (CD46) protects cells predominantly from alternative complement pathway-mediated C3-fragment deposition and cytolysis. *J Immunol* 1993; **151**: 1519–1527.

9 Medof ME, Kinoshita T, Nussenzweig V. Inhibition of complement activation on the surface of cells after incorporation of decay-accelerating factor (DAF) into their membranes. *J Exp Med* 1984; **160**: 1558–1578.

10 Meri S, Morgan BP, Davies A, Daniels RH, Olavesen MG, Waldmann H *et al.* Human protectin (CD59), an 18,000-20,000 MW complement lysis restricting factor, inhibits C5b-8 catalysed insertion of C9 into lipid bilayers. *Immunology* 1990; **71**: 1–9.

11 Roumenina LT, Daugan MV, Petitprez F, Sautès-Fridman C, Fridman WH. Context-dependent roles of complement in cancer. *Nat Rev Cancer* 2019; **19**: 698–715.

12 Weiner GJ. Rituximab: mechanism of action. *Semin Hematol* 2010; **47**: 115–123.

13 Cragg MS, Morgan SM, Chan HTC, Morgan BP, Filatov AV, Johnson PWM *et al.* Complement-mediated lysis by anti-CD20 mAb correlates with segregation into lipid rafts. *Blood* 2003; **101**: 1045–1052.

14 Golay J, Taylor RP. The Role of Complement in the Mechanism of Action of Therapeutic Anti-Cancer mAbs. *Antibodies (Basel)* 2020; **9**. doi:10.3390/antib9040058.

15 Hu W, Ge X, You T, Xu T, Zhang J, Wu G *et al.* Human CD59 inhibitor sensitizes rituximab-resistant lymphoma cells to complement-mediated cytolysis. *Cancer Res* 2011; **71**: 2298–2307.

16 Du Y, Teng X, Wang N, Zhang X, Chen J, Ding P *et al.* NF-κB and enhancer-binding CREB protein scaffolded by CREB-binding protein (CBP)/p300 proteins regulate CD59

protein expression to protect cells from complement attack. *J Biol Chem* 2014; **289**: 2711–2724.

17 Kurosawa G, Akahori Y, Morita M, Sumitomo M, Sato N, Muramatsu C *et al.* Comprehensive screening for antigens overexpressed on carcinomas via isolation of human mAbs that may be therapeutic. *Proc Natl Acad Sci U S A* 2008; **105**: 7287–7292.

18 Geller A, Yan J. The Role of Membrane Bound Complement Regulatory Proteins in Tumor Development and Cancer Immunotherapy. *Front Immunol* 2019; **10**: 440775.

19 Candelaria M, Dueñas-Gonzalez A. Rituximab in combination with cyclophosphamide, doxorubicin, vincristine, and prednisone (R-CHOP) in diffuse large B-cell lymphoma. *Ther Adv Hematol* 2021; **12**: 2040620721989579.

20 van Meerten T, van Rijn RS, Hol S, Hagenbeek A, Ebeling SB. Complement-induced cell death by rituximab depends on CD20 expression level and acts complementary to antibody-dependent cellular cytotoxicity. *Clin Cancer Res* 2006; **12**: 4027–4035.

21 Macor P, Tripodo C, Zorzet S, Piovan E, Bossi F, Marzari R *et al.* In vivo targeting of human neutralizing antibodies against CD55 and CD59 to lymphoma cells increases the antitumor activity of rituximab. *Cancer Res* 2007; **67**: 10556–10563.

22 Naniche D, Varior-Krishnan G, Cervoni F, Wild TF, Rossi B, Rabourdin-Combe C *et al.* Human membrane cofactor protein (CD46) acts as a cellular receptor for measles virus. *J Virol* 1993; **67**: 6025–6032.

23 Sleiman SF, Langley BC, Basso M, Berlin J, Xia L, Payappilly JB *et al.* Mithramycin is a gene-selective Sp1 inhibitor that identifies a biological intersection between cancer and neurodegeneration. *J Neurosci* 2011; **31**: 6858–6870.

24 Martin BK. Transcriptional control of complement receptor gene expression. *Immunol Res* 2007; **39**: 146–159.

25 Torabi B, Flashner S, Beishline K, Sowash A, Donovan K, Bassett G *et al.* Caspase cleavage of transcription factor Sp1 enhances apoptosis. *Apoptosis* 2018; **23**: 65–78.

26 Yu B, Datta PK, Bagchi S. Stability of the Sp3-DNA complex is promoter-specific: Sp3 efficiently competes with Sp1 for binding to promoters containing multiple Sp-sites. *Nucleic Acids Res* 2003; **31**: 5368–5376.

27 Mok GF, Folkes L, Weldon SA, Maniou E, Martinez-Heredia V, Godden AM *et al.* Characterising open chromatin in chick embryos identifies cis-regulatory elements important for paraxial mesoderm formation and axis extension. *Nat Commun* 2021; **12**: 1–15.

28 Wang M, Qiu L, Ru X, Song Y, Zhang Y. Distinct isoforms of Nrf1 diversely regulate different subsets of its cognate target genes. *Sci Rep* 2019; **9**: 1–15.

29 Friedman AD. Transcriptional control of granulocyte and monocyte development. *Oncogene* 2007; **26**: 6816–6828.

30 Jiang Y, Mu H, Zhao H. HMBOX1, a member of the homeobox family: current research progress. *Cent Eur J Immunol* 2023; **48**: 63–69.

31 Li D-Q, Pakala SB, Reddy SDN, Ohshiro K, Zhang J-X, Wang L *et al*. Bidirectional autoregulatory mechanism of metastasis-associated protein 1-alternative reading frame pathway in oncogenesis. *Proc Natl Acad Sci U S A* 2011; **108**: 8791–8796.

32 Golay J, Zaffaroni L, Vaccari T, Lazzari M, Borleri G-M, Bernasconi S *et al*. Biologic response of B lymphoma cells to anti-CD20 monoclonal antibody rituximab in vitro: CD55 and CD59 regulate complement-mediated cell lysis. *Blood* 2000; **95**: 3900–3908.

33 Olofsson BA, Kelly CM, Kim J, Hornsby SM, Azizkhan-Clifford J. Phosphorylation of Sp1 in response to DNA damage by ataxia telangiectasia-mutated kinase. *Mol Cancer Res* 2007; **5**: 1319–1330.

34 O'Connor L, Gilmour J, Bonifer C. The role of the ubiquitously expressed transcription factor Sp1 in tissue-specific transcriptional regulation and in disease. *Yale J Biol Med* 2016; **89**: 513–525.

35 Suske G. The Sp-family of transcription factors. *Gene* 1999; **238**: 291–300.

36 Jiang K, Deng M, Du W, Liu T, Li J, Zhou Y. Functions and inhibitors of CHK1 in cancer therapy. *Med Drug Discov* 2024; **22**: 100185.

37 Kristeleit R, Plummer R, Jones R, Carter L, Blagden S, Sarker D *et al.* A Phase 1/2 trial of SRA737 (a Chk1 inhibitor) administered orally in patients with advanced cancer. *Br J Cancer* 2023; **129**: 38–45.

38 Jones R, Plummer R, Moreno V, Carter L, Roda D, Garralda E *et al.* A Phase I/II trial of oral SRA737 (a Chk1 inhibitor) given in combination with low-dose gemcitabine in patients with advanced cancer. *Clin Cancer Res* 2023; **29**: 331–340.

39 Fan Z, Luo H, Zhou J, Wang F, Zhang W, Wang J *et al.* Checkpoint kinase□1 inhibition and etoposide exhibit a strong synergistic anticancer effect on chronic myeloid leukemia cell line K562 by impairing homologous recombination DNA damage repair. *Oncol Rep* 2020; **44**: 2152–2164.

40 Isono M, Okubo K, Asano T, Sato A. Inhibition of checkpoint kinase 1 potentiates anticancer activity of gemcitabine in bladder cancer cells. *Sci Rep* 2021; **11**: 10181.

41 Giang J, Seelen MAJ, van Doorn MBA, Rissmann R, Prens EP, Damman J. Complement activation in inflammatory skin diseases. *Front Immunol* 2018; **9**: 639.

42 Petr V, Thurman JM. The role of complement in kidney disease. *Nat Rev Nephrol* 2023; **19**: 771–787.

43 Sina C, Kemper C, Derer S. The intestinal complement system in inflammatory bowel disease: Shaping intestinal barrier function. *Semin Immunol* 2018; **37**: 66–73.

44 Kolev M, Das M, Gerber M, Baver S, Deschatelets P, Markiewski MM. Inside-out of complement in cancer. *Front Immunol* 2022; **13**: 931273.

45 Trabolsi A, Arumov A, Schatz JH. Bispecific antibodies and CAR-T cells: dueling immunotherapies for large B-cell lymphomas. *Blood Cancer J* 2024; **14**: 27.

46 Bulla R, Tripodo C, Rami D, Ling GS, Agostinis C, Guarnotta C *et al*. C1q acts in the tumour microenvironment as a cancer-promoting factor independently of complement activation. *Nat Commun* 2016; **7**: 10346.

47 Stadlbauer K, Andorfer P, Stadlmayr G, Rüker F, Wozniak-Knopp G. Bispecific mAb2 antibodies targeting CD59 enhance the complement-dependent cytotoxicity mediated by rituximab. *Int J Mol Sci* 2022; **23**: 5208.

48 Cox J, Mann M. MaxQuant enables high peptide identification rates, individualized p.p.b.-range mass accuracies and proteome-wide protein quantification. *Nat Biotechnol* 2008; **26**: 1367–1372.

49 Cox J, Hein MY, Luber CA, Paron I, Nagaraj N, Mann M. Accurate proteome-wide label-free quantification by delayed normalization and maximal peptide ratio extraction, termed MaxLFQ. *Mol Cell Proteomics* 2014; **13**: 2513–2526.

50 Darrah PA, Patel DT, De Luca PM, Lindsay RWB, Davey DF, Flynn BJ *et al*. Multifunctional TH1 cells define a correlate of vaccine-mediated protection against Leishmania major. *Nat Med* 2007; **13**: 843–850.

51 Manso BA, Medina KL. Standardized flow-cytometry-based protocol to simultaneously measure transcription factor levels. *STAR Protoc* 2021; **2**: 100485.

52 Posit. Posit. 2022.https://posit.co/ (accessed 17 Sep2024).

53 Perez-Riverol Y, Bai J, Bandla C, García-Seisdedos D, Hewapathirana S, Kamatchinathan S *et al.* The PRIDE database resources in 2022: a hub for mass spectrometry-based proteomics evidences. *Nucleic Acids Res* 2022; **50**: D543–D552.

Acknowledgements:
We thank Michelle Mok Meng Huang and Erica Xu Songci from the Fluorescence Activated Cell Sorting Facility at CSI for maintenance of flow cytometry machines and guidance on flow cytometry analysis. We thank Choong Meng Ling from the Experimental Drug Development Centre at A*STAR for assistance in the design of the chemical screen. We thank Giridharan Periyasamy, Matan Thangavelu, and Shivaji Rikka from Center for High-throughput Phenomics, Genome Institute of Singapore for providing access to the high-throughput screening facility and drug libraries, and discussion on design of chemical screen. We thank Dr. Joseph J Zhao from the Yong Loo Lin School of Medicine, National University of Singapore for assistance with Rstudio Fig.s. We acknowledge the generous gift of the CD46 hybridoma from Dr. Denis Gerlier (INSERM), contributed through the CelluloNet facility of UMS3444/USB Biosciences Gerland-Lyon Sud.

Funding:
Experimental Drug Development Centre through the Target Translation Consortium initiative (project number: TTC2019_003) (ADJ)
Singapore Ministry of Health’s National Medical Research Council Clinician Scientist Award (CSAINV20nov-0010) (ADJ)

National Medical Research Council Open Fund Large Collaborative Grant, (SYMPHONY; NMRC OF-LCG18May-0028) (ADJ)
Cancer Science Institute of Singapore, National University of Singapore through the National Research Foundation Singapore (ADJ)
Singapore Ministry of Education under its Research Centres of Excellence initiative (ADJ)

Author contributions:
Conceptualization: ASYC, ADJ
Methodology: ASYC, WKY, VK, LJM, NM, DK, ADJ
Validation: ASYC, AA, CZYO, MMH, NM, MIBA, GH
Formal analysis: ASYC, VK
Investigation: ASYC, AA, CZYO, MMH, NM, GH, ADJ
Resources: PMH
Writing – Original Draft: ASYC, ADJ
Writing – Review & Editing: ASYC, PWJ, CZYO, WKY, NM, PMH, MSC, WJC, MSC, DK, CT, ADJ
Visualization: ASYC, VK
Supervision: ADJ
Project administration: PWJ, ADJ
Funding acquisition: ADJ

Competing Interests:
ADJ has received consultancy fees from DKSH/Beigene, Roche, Gilead, Turbine Ltd, AstraZeneca, Antengene, Janssen, MSD and IQVIA; and research funding from Janssen and AstraZeneca. MSC is a retained consultant for BioInvent International and has performed educational and advisory roles for Baxalta and Boehringer Ingleheim. He has consulted for GSK, Radiant, iTeos Therapeutics, Surrozen, Hanall, Argenx and Mestag and received research funding from BioInvent, Surrozen, GSK, UCB and iTeos.

Data and materials availability:
All data relevant to the study are included in the article or uploaded as online supplemental information. The mass spectrometry data have been deposited to the ProteomeXchange Consortium via the PRIDE partner repository with the dataset identifier PXD056654 [53].

Figure Legends:

Fig. 1. ICOS Screen identifies upregulation of CD46 as response to DNA damage

(A) Schematic illustration of the multi-stage process of the phage-display antibody screen used to identify antibodies that preferentially bind to DNA-damaged cells.
(B) Flow cytometry histogram of CD46 levels in MCF10A cells exposed to various doses of irradiation (0, 2, 5, 10 Gy) and stained with PE-conjugated anti-CD46 antibody or IgG-PE as isotype control.

(C) Flow cytometry histogram of CD46 levels in SUDHL4 cells treated with various chemotherapy for 48H. Conditions include untreated control, IgG-PE isotype control, and treatments with 1uM etoposide (ETO), 10nM gemcitabine (GEM), 0.2mM Hydroxyurea (HU), and 2nM vincristine (VCR).
(D) Representative flow cytometry histograms of CD46, CD55, and CD59 in SUDHL4 cells treated with or without etoposide (ETO). Cells were stained with PE-conjugated specific antibodies or IgG-PE as isotype control.
(E) Quantification of relative integrated mean fluorescence intensities (iMFI) for CD46, CD55, and CD59 in SUDHL4 cells treated with ETO, normalized to untreated control. Statistical analysis was performed using ratio paired t-tests of IgG-corrected iMFI values. Data are presented as mean ± SD from three independent experiments. Statistical significance is denoted as follows: * $p < 0.05$, ** $p < 0.01$, *** $p < 0.001$.

Fig. 2. Chemotherapy prevents rituximab-induced CDC via upregulation of CD59

(A) Mean cell viability of 10 DLBCL cell lines treated with 10 ug/mL rituximab (RTX) over 2 hours, measured by CTG assay. Black dots represent CDC-mediated cell death, while clear dots indicate RTX-induced direct cell death. Error bars represent SD ($n \geq 2$ biological replicates).
(B) Heatmap showing log-transformed normalized transcript per million (nTPM) RNA expression values for CD20, CD46, CD55, and CD59 in DLBCL cell lines, obtained from The Human Protein Atlas, ranked by %CDC activity derived from Fig. 2B.
(C) Dose-response curve of RTX-induced cell death in SUDHL4 cells pre-treated with etoposide (ETO) for 48H, measured by CTG assay. HS, human serum; hiHS, heat-inactivated human serum. Data fitted using a four-parameter variable slope model (n=3 biological replicates).
(D) Cell death induced by RTX (37 ng/mL) in SUDHL4 cells pre-treated with various chemotherapeutic agents: doxorubicin (DOX), etoposide (ETO), gemcitabine (GEM), hydroxyurea (HU), and vincristine (VCR) for 48H. Both CDC and direct cell death are shown (n=3 biological replicates). Statistical significance was calculated by 2-way ANOVA relative to respective control followed by uncorrected Fisher's LSD. Significance of % CDC and not % apoptosis is shown.
(E) Representative flow cytometry histogram of CD20 expression in SUDHL4 cells treated with or without ETO. Cells were stained with APC-conjugated anti-CD20 antibody or IgG-APC as isotype control.
(F) Relative mean fluorescence intensity (MFI) of CD20 in SUDHL4 cells treated with ETO, normalized to untreated control (n=4 biological replicates). Statistical significance was calculated by ratio paired t-test of IgG-corrected MFI values.
(G) Percentage of CDC in SUDHL4 cells treated with 37 ng/mL RTX including ETO-treated with blocking antibodies against CD46, CD55, or CD59 (n=3 biological replicates). Statistical significance among groups was determined using a mixed effect model, followed by post hoc Dunnett's multiple comparisons test. Data are presented as mean ± SD. Statistical significance is denoted as follows: * $p < 0.05$, ** $p < 0.01$, *** $p < 0.001$.

Fig. 3. Kinase Library Drug Screen identifies Chk1 as therapeutic target to recover rituximab CDC efficacy

(A) Schematic diagram illustrating the kinase library drug screen CDC procedure.
(B) Pie chart depicting the distribution of targeted pathways in the 418 Selleckchem Kinase Library.
(C) Ranked dot plot of kinase library screen hits, showing log % cell viability (CV) of etoposide-treated cells normalized to control. The dotted line indicates the 5th percentile threshold.
(D) Nested pie chart illustrating the targeted pathways and corresponding protein targets among the hits below the 5th percentile.
(E) Fold change of % CDC (normalized to control) in SUDHL4 cells treated with etoposide (ETO) and various ATR or Chk1 inhibitors (n=3 biological replicates).
(F, G) % CDC in SUDHL4 (F) and SUDHL6 (G) cells pretreated with indicated compounds, including the Chk1 inhibitor Rabusertib, for 48 hours. For panels E-G, statistical significance was calculated by mixed-effects model with Dunnett's multiple comparisons test relative to the ETO condition. Error bars represent SD of biological replicates. Statistical significance is denoted as follows: * $p < 0.05$, ** $p < 0.01$, *** $p < 0.001$.

Fig. 4. Chk1 is responsible for DDR-regulated mCRP expression

(A) Immunoblot of Chk1 and phosphorylated Chk1 Ser345 (pChk1) in SUDHL4 cells treated with or without etoposide (ETO) for 48 hours.
(B) Bar chart showing relative integrated mean fluorescence intensity (iMFI) of CD46, CD55, and CD59 in SUDHL4 cells treated with ETO alone or ETO + Chk1 inhibitor (Chk1i, Rabusertib). Statistical analysis was performed using repeated measures one-way ANOVA with Dunnett's multiple comparisons test relative to the ETO condition. Error bars represent SD of 4 biological replicates. Statistical significance is denoted as follows: * $p < 0.05$, ** $p < 0.01$, *** $p < 0.001$.
(C) Representative flow cytometry histograms in Fig. 4B of CD46, CD55, and CD59 expression in SUDHL4 cells under control conditions, ETO treatment, or ETO + Chk1i treatment. Cells were stained with PE-conjugated specific antibodies or IgG-PE as isotype control.
(D) Flow cytometry histograms of CD59 expression in multiple DLBCL cell lines (SUDHL6, SUDHL2, Karpas-231) under control conditions, ETO treatment, or ETO + Chk1i treatment. Cells were stained with PE-conjugated anti-CD59 antibody or IgG-PE as isotype control.

Fig. 5. Etoposide-induced *CD59* gene expression is rescued with Mithramycin A

(A-C) Relative mRNA expression of *CD46* (A), *CD55* (B), and *CD59* (C) in SUDHL4 cells treated with etoposide (ETO) or ETO + Chk1 inhibitor (Chk1i, Rabusertib).
(D) Schematic diagram of *CD59* gene transcriptional regulators (adapted from Du et al.).
(E) Sp1 and NF-κB primarily regulate transcripts T1-T4. TP53 regulates the T5 transcript but has minimal impact on overall CD59 expression. CREB primarily regulates T6-T8 transcripts

and plays additional roles in CD59 transcription beyond T6-T8 regulation. An enhancer region (-500 to -1000 bp) interacts with multiple factors (CREB, NF-κB, TP53) through CBP/p300 scaffolding, facilitating coordinated regulation of CD59 expression. (E) Relative mRNA expression of *CD59* exons T1-4, T5, and T6-8 in SUDHL4 cells after ETO or ETO + Chk1i treatment.

(F) Percentage of complement-dependent cytotoxicity (%CDC) in SUDHL4 cells pretreated with ETO or ETO + 10 nM Mithramycin A (MitA).

(G,H) Bar chart showing CD59 protein levels (MFI relative to control) (G) and relative *CD59* mRNA expression (H) in SUDHL4 cells treated with control, ETO, or ETO + 10 nM MitA.

(I) Immunoblot analysis of Sp1 protein and cleaved caspase-3 in SUDHL4 cells after treatment with indicated compounds. For all panels, statistical significance was calculated by ANOVA followed by post hoc Dunnett's multiple comparisons test relative to the ETO condition. Error bars represent SD of biological replicates. Statistical significance is denoted as follows: * $p < 0.05$, ** $p < 0.01$, *** $p < 0.001$.

Fig. 6. Etoposide treatment induces Chk1-dependent changes to the Sp1 interactome

(A) Schematic diagram of co-immunoprecipitation mass spectrometry workflow. SUDHL4 cells were treated under three conditions (CTRL, ETO, ETO + Chk1i (Rabusertib)) for 48 hours in 4 biological replicates. Nuclear lysates were extracted and incubated with either Sp1 antibody (EPR22648) or rabbit IgG. Protein A beads were used to pull down antibody-protein complexes, followed by protein elution and label-free quantification mass spectrometry (LFQ-MS) analysis.

(B-D) Volcano plots showing enriched Sp1-bound proteins compared to IgG control for CTRL (B), ETO (C), and ETO+Chk1i (D) conditions in SUDHL4 cells. Significant hits are noted based on a two-dimensional cut-off with log2FC> 2 and –log10 p-values > 2. Error bars represent the standard deviations from three iterations of zero-value imputation.

(E) Heatmap of proteins significantly enriched by Sp1 vs IgG in any of three conditions in SUDHL4 cells, and categorized as transcription factors, epigenetic complex, or other nuclear proteins.

(F) Heatmap of proteins that met criteria: |delta_log2FE_ETO_vs_CTRL| > 2, and delta_log2FE_ETO_vs_CTRL and delta_log2FE_ETO_vs_ETO+Chk1i are both positive or both negative.

(G-H) STRING protein interaction network of selected proteins in Fig. 6F (G) and in Fig. 6E (only proteins connected to SP1 is shown, H). Lines indicate confidence level from both functional and physical protein associations, with sources based from experiments of databases. Minimum required interaction score was 0.15.

Fig. 7. Illustration of chemotherapy-induced rituximab antagonism via CD59 upregulation

Schematic representation of the mechanism by which genotoxic agents antagonize rituximab-mediated complement-dependent cytotoxicity (CDC) through CD59 upregulation. Left panel:

Under normal conditions, rituximab can induce CDC, resulting in membrane attack complex (MAC) formation and cell lysis. CD59 expression is driven by Sp1 and regulated by repressor complexes. Right panel: In the presence of DNA damage, genotoxic agents activate Chk1. Activated Chk1 prevents repressor complexes from associating with Sp1-bound promoter sites. Unrestricted Sp1 drives increased mCRP gene expression, particularly CD59. Elevated CD59 levels block MAC formation, inhibiting rituximab-driven CDC.

Supplementary Materials and Methods

Antibodies	Source	Identifier
Anti-cleaved caspase 3 (Asp 175), rabbit polyclonal	Cell Signaling Technology	9661
Anti-Chk1, mouse monoclonal	Cell Signaling Technology	2360
Anti-pChk1 Ser345, rabbit monoclonal	Cell Signaling Technology	2348
Anti-SP1 antibody [EPR22648-50] - ChIP Grade, rabbit monoclonal	Abcam	ab231778
Anti-SP1 antibody [E-3], mouse monoclonal	Santa Cruz Biotechnology	sc-17824
Anti-SP1 antibody, rabbit polyclonal	Proteintech	21962-1-AP
APC Mouse Anti-Human CD20	BD Bioscience	559776
APC Mouse Anti-Human CD20	BD Bioscience	559776
APC Mouse IgG1, κ Isotype Control	BD Bioscience	555751
CD46 (MC120.6)	SFR Biosciences	
CD55 (BRI216)	Bio-Rad	MCA914
CD59 (YTH53.1)	Bio-Rad	MCA715G
PE Mouse Anti-Human CD46	BD Bioscience	564252
PE Mouse Anti-Human CD55	BD Bioscience	341030
PE Mouse Anti-Human CD59	BD Bioscience	555764
PE Mouse IgG2a, κ Isotype Control	BD Bioscience	553457
Rabbit IgG Isotype Control	Invitrogen	02-6102

Compound Name	Source	Identifier
CCT244747	MedChemExpress	HY-18175
CPI-637	MedChemExpress	HY-100482
Curcumin	MedChemExpress	HY-N0005
Dexamethasone	MedChemExpress	HY-14648
Doxorubicin	MedChemExpress	HY-15142
Etoposide	MedChemExpress	HY-13629
Gemcitabine	MedChemExpress	HY-17026
Hydroxyurea	Sigma-Aldrich	H8627
JSH-23	MedChemExpress	HY-13982
Mithramycin A	Sigma-Aldrich	M6891
MK-8776	MedChemExpress	HY-15532

MLN120B	MedChemExpress	HY-15473
QNZ	MedChemExpress	HY-13812
Rabusertib	MedChemExpress	HY-14720
VE-821	MedChemExpress	HY-14731
Vincristine	Adooq Bioscience	A10973

Primer Target	Forward primer (5'->3')	Reverse primer (5'->3')
18S	GTAACCCGTTGAACCCATT	CCATCCAATCGGTAGTAGCG
CD20	GAGCCAATGAAAGGCCCTATT	AAGAAGCTTTGCGTGGGGCC
CD46	GCGCTTTCCTGGGTTGCT	ACAGGCATCGGAGAAGTAC
CD55	TTCCCGCAGATGTACCTAATGC	TTACAGTATCCTCGGGAAAACT
CD59 (T1-T8)	GATGCGTGTCTCATTACCAA	AAGGATGTCCCACCATTTTC
CD59 (T1-T4)	AGGCTGGAAGAGGATCTTGG	AGGCTATGACCTGAATGGCA
CD59 (T5)	CTTACAGTGAGGAGCCAGAG	AATGAGACACGCATCAAAAT
CD59 (T6-T8)	TGACTCACTGACCCTGATGGG	CTATGACCTGAATGGCAGAAGA

Figure S1. Phage-display Antibody Screen Design

Schematic illustration of the multi-stage process of the phage-display antibody screen used to identify antibodies that preferentially bind to DNA-damaged cells.
(A) The process begins with the construction of the phage-display antibody library, which includes generating a diverse library of antibody sequences, cloning these sequences, and producing the antibody phage library.
(B) In the initial screening step, cells exposed to the phage library were treated with an organic solvent and sedimented to remove non-specific binders. The phage library was then exposed to undamaged MCF10A cells, and the binders obtained through ICOS (Immunoprecipitation of Crosslinked and Sonicated) were converted into a masking antibody set for MCF10A cells.
(C) The final stage involves the screening of DNA damage-specific binders. In this step, irradiated MCF10A cells were treated with the masking antibody set and then exposed to the phage library to obtain phage complexes by ICOS that preferentially bind DNA-damaged cells. To validate the results, scFv fragments were purified from 20 selected phage complexes and tested by flow cytometry to select the best candidates based on consistency of DNA damage-related induction. This phage-display screen design allows for the identification of antibodies that specifically recognize epitopes present or upregulated in DNA-damaged cells while minimizing binding to undamaged cells.

Figure S2. Chemotherapy Cell Viability

(A) Cell viability of SUDHL4 cells treated with indicated doses of compounds for 48 hours in technical triplicate.

Figure S3. MC120.6 CD46 Blocking Antibody Validation

(A) Schematic illustrating the complement-dependent cytotoxicity (CDC) assay protocol.
(B) Flow cytometry histogram of SUDHL4 cells stained with a control mouse IgGκ primary antibody followed with a secondary anti-mouse AlexaFluor 488, and the CD46 (MC120.6) antibody followed with a secondary anti-mouse AlexaFluor 488.
(C) Flow cytometry histogram of ETO-treated SUDHL4 cells stained with conjugated CD46-PE antibody, or blocked with CD46 (MC120.6) followed by staining with conjugated CD46-PE antibody.

Figure S4. Etoposide-induced *CD59* gene expression is rescued with Mithramycin A

(A) Relative mRNA expression of *CD59* exons T1-8, T1-4, T5, and T6-8 in SUDHL6 cells after ETO or ETO + Chk1i treatment.
(B) Percentage of CDC in SUDHL4 cells treated with indicated NF-κB inhibitors for 48 hours. (n=3 technical triplicates).
(C) Percentage of CDC in SUDHL6 cells pretreated with etoposide (ETO) alone or in combination with Mithramycin A (MitA) (n=3 biological replicates).
(D) Relative CD46 expression in SUDHL4 cells treated with etoposide alone or in combination with Mithramycin A (n=2 biological replicates).
(E) Flow cytometry histogram of SUDHL4 cells treated with or without Mithramycin A, showing IgG-PE control and CD46-PE staining. Statistical analysis for all panels was performed using one-way ANOVA followed by Dunnett's multiple comparisons test, with the etoposide-treated condition as the reference group. Error bars represent standard deviation. Statistical significance is denoted as follows: * $p < 0.05$, ** $p < 0.01$, *** $p < 0.001$.

Figure S5. Etoposide treatment induces Chk1-dependent changes to the Sp1 interactome

(A) Heatmap of log2 LFQ intensity of proteins significantly enriched (log2FC> 2 and –log10 p-values > 2) in any of the 3 analyses are plotted using z-score.
(B) Log2FC of significantly enriched non-nuclear proteins.

Figure 1

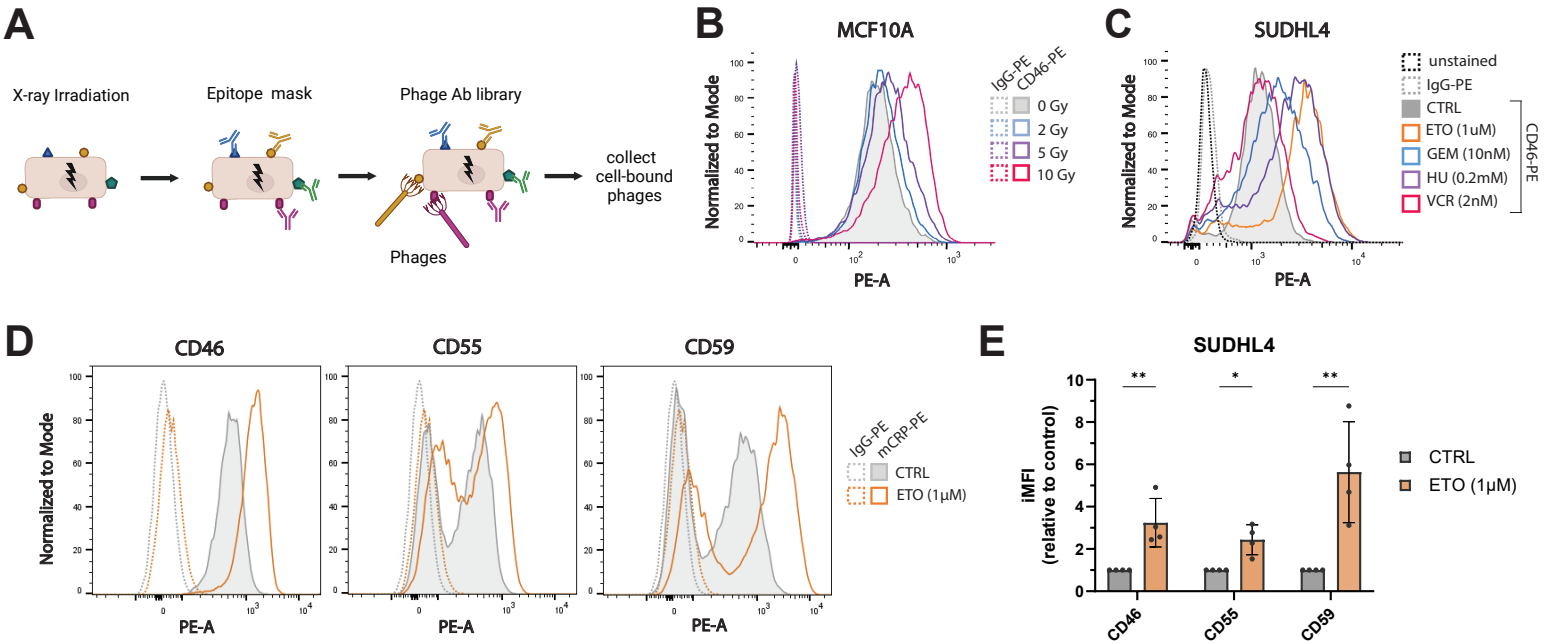
A
X-ray Irradiation
Epitope mask
Phage Ab library
Phages
collect cell-bound phages
B
MCF10A
Normalized to Mode
PE-A
IgG-PE
CD46-PE
0 Gy
2 Gy
5 Gy
10 Gy
C
SUDHL4
Normalized to Mode
PE-A
unstained
IgG-PE
CTRL
ETO (1uM)
GEM (10nM)
HU (0.2mM)
VCR (2nM)
CD46-PE
D
CD46
CD55
CD59
Normalized to Mode
PE-A
IgG-PE
mCRP-PE
CTRL
ETO (1μM)
E
SUDHL4
iMFI (relative to control)
CD46
CD55
CD59
CTRL
ETO (1μM)

Figure 2

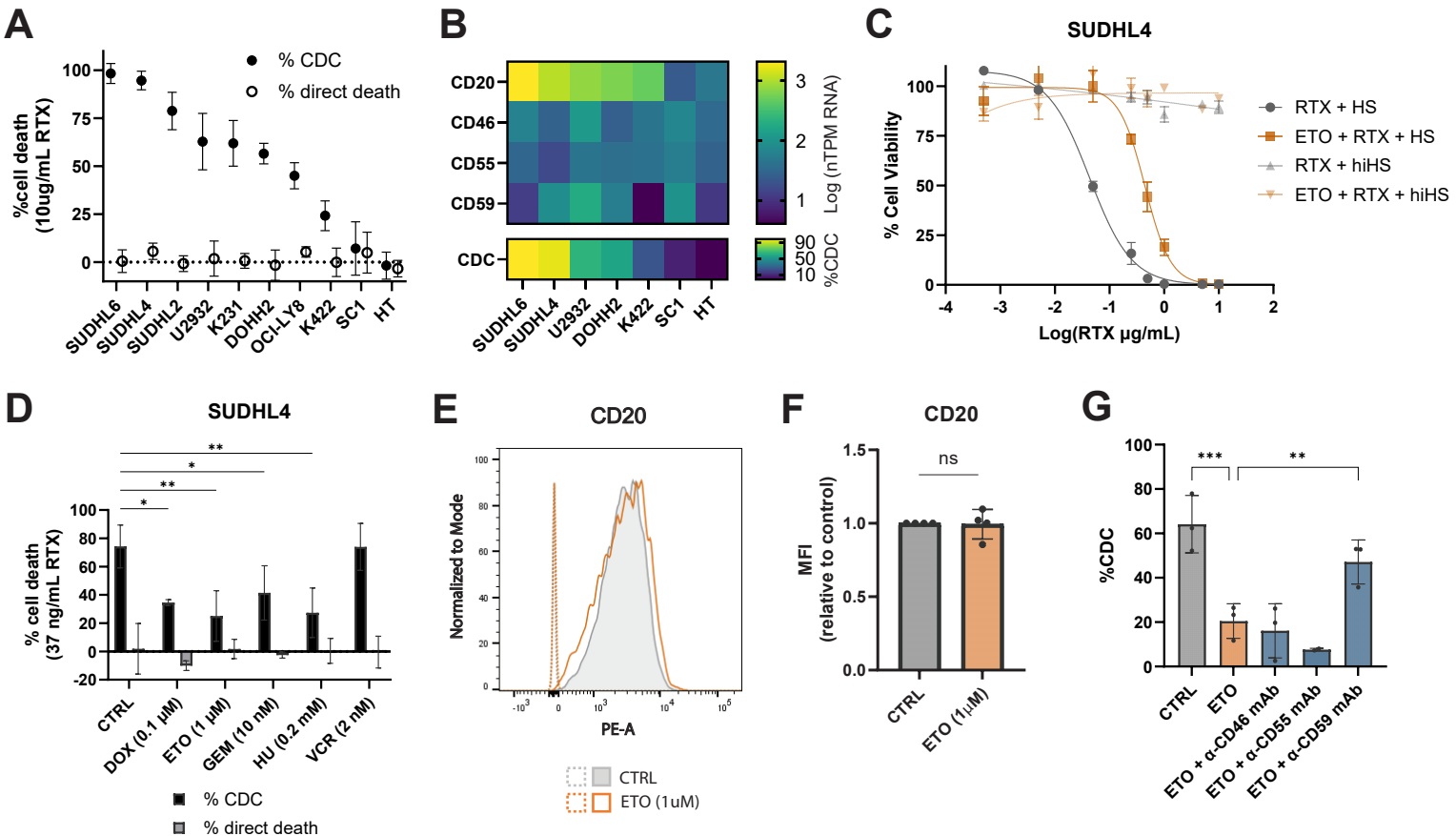
A
% CDC
% direct death
%cell death (10ug/mL RTX)
100
75
50
25
0
SUDHL6
SUDHL4
SUDHL2
U2932
K231
DOHH2
OCI-LY8
K422
SC1
HT
B
CD20
CD46
CD55
CD59
CDC
3
2
1
Log (nTPM RNA)
90
50
10
%CDC
C
SUDHL4
% Cell Viability
Log(RTX µg/mL)
RTX + HS
ETO + RTX + HS
RTX + hiHS
ETO + RTX + hiHS
D
SUDHL4
% cell death (37 ng/mL RTX)
CTRL
DOX (0.1 µM)
ETO (1 µM)
GEM (10 nM)
HU (0.2 mM)
VCR (2 nM)
% CDC
% direct death
E
CD20
Normalized to Mode
PE-A
CTRL
ETO (1uM)
F
CD20
MFI (relative to control)
ns
CTRL
ETO (1µM)
G
%CDC
***
**
CTRL
ETO
ETO + α-CD46 mAb
ETO + α-CD55 mAb
ETO + α-CD59 mAb

Figure 3

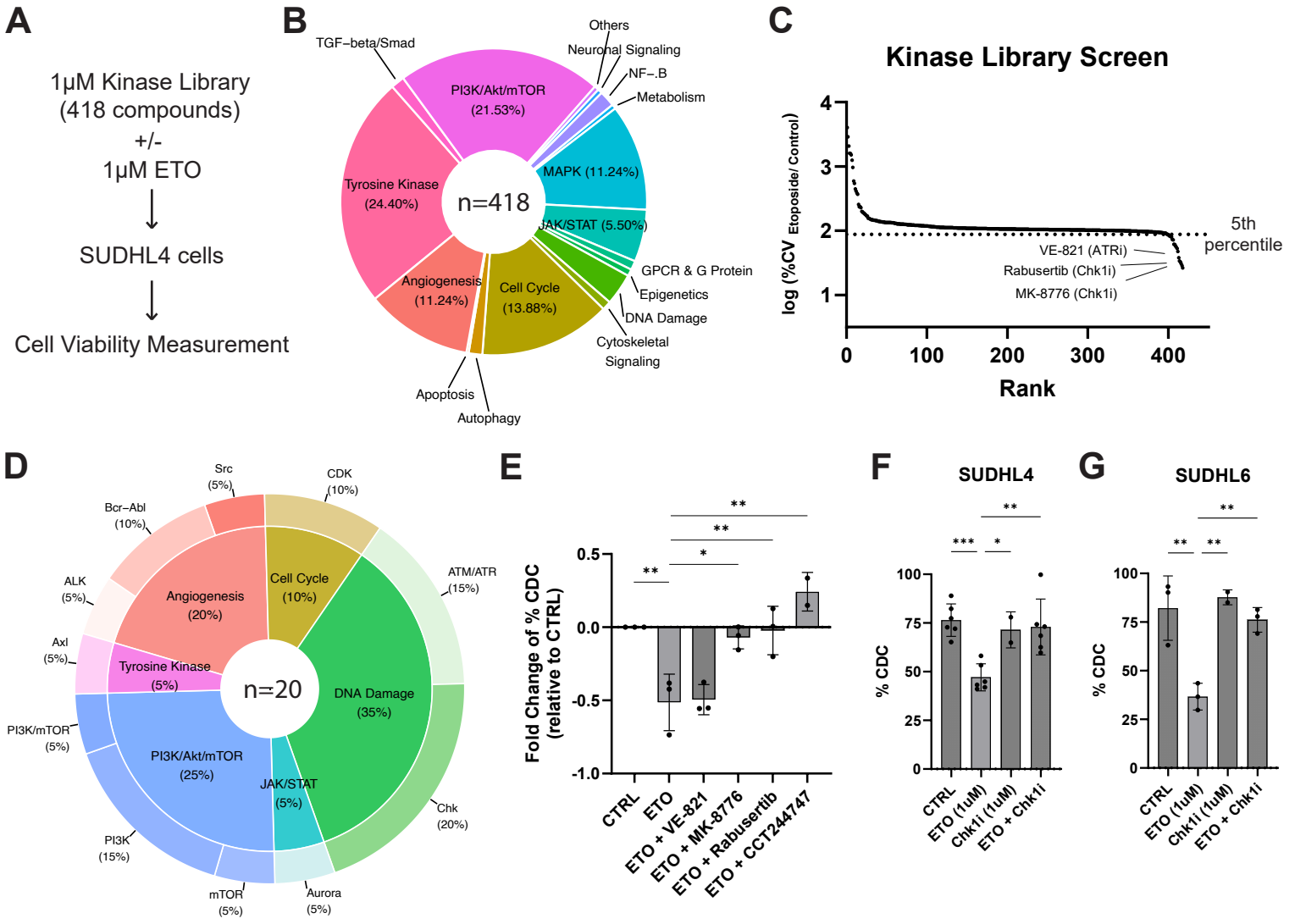
A
1μM Kinase Library
(418 compounds)
+/-
1μM ETO
SUDHL4 cells
Cell Viability Measurement
B
n=418
PI3K/Akt/mTOR (21.53%)
MAPK (11.24%)
JAK/STAT (5.50%)
Cell Cycle (13.88%)
Angiogenesis (11.24%)
Tyrosine Kinase (24.40%)
TGF−beta/Smad
Others
Neuronal Signaling
NF−.B
Metabolism
GPCR & G Protein
Epigenetics
DNA Damage
Cytoskeletal Signaling
Apoptosis
Autophagy
C
Kinase Library Screen
log (%CV Etoposide/ Control)
Rank
5th percentile
VE-821 (ATRi)
Rabusertib (Chk1i)
MK-8776 (Chk1i)
D
n=20
Angiogenesis (20%)
Cell Cycle (10%)
DNA Damage (35%)
JAK/STAT (5%)
PI3K/Akt/mTOR (25%)
Tyrosine Kinase (5%)
Src (5%)
CDK (10%)
Bcr−Abl (10%)
ALK (5%)
Axl (5%)
PI3K/mTOR (5%)
PI3K (15%)
mTOR (5%)
Aurora (5%)
Chk (20%)
ATM/ATR (15%)
E
Fold Change of % CDC (relative to CTRL)
CTRL
ETO
ETO + VE-821
ETO + MK-8776
ETO + Rabusertib
ETO + CCT244747
F
SUDHL4
% CDC
CTRL
ETO (1uM)
Chk1i (1uM)
ETO + Chk1i
G
SUDHL6
% CDC
CTRL
ETO (1uM)
Chk1i (1uM)
ETO + Chk1i

Figure 4

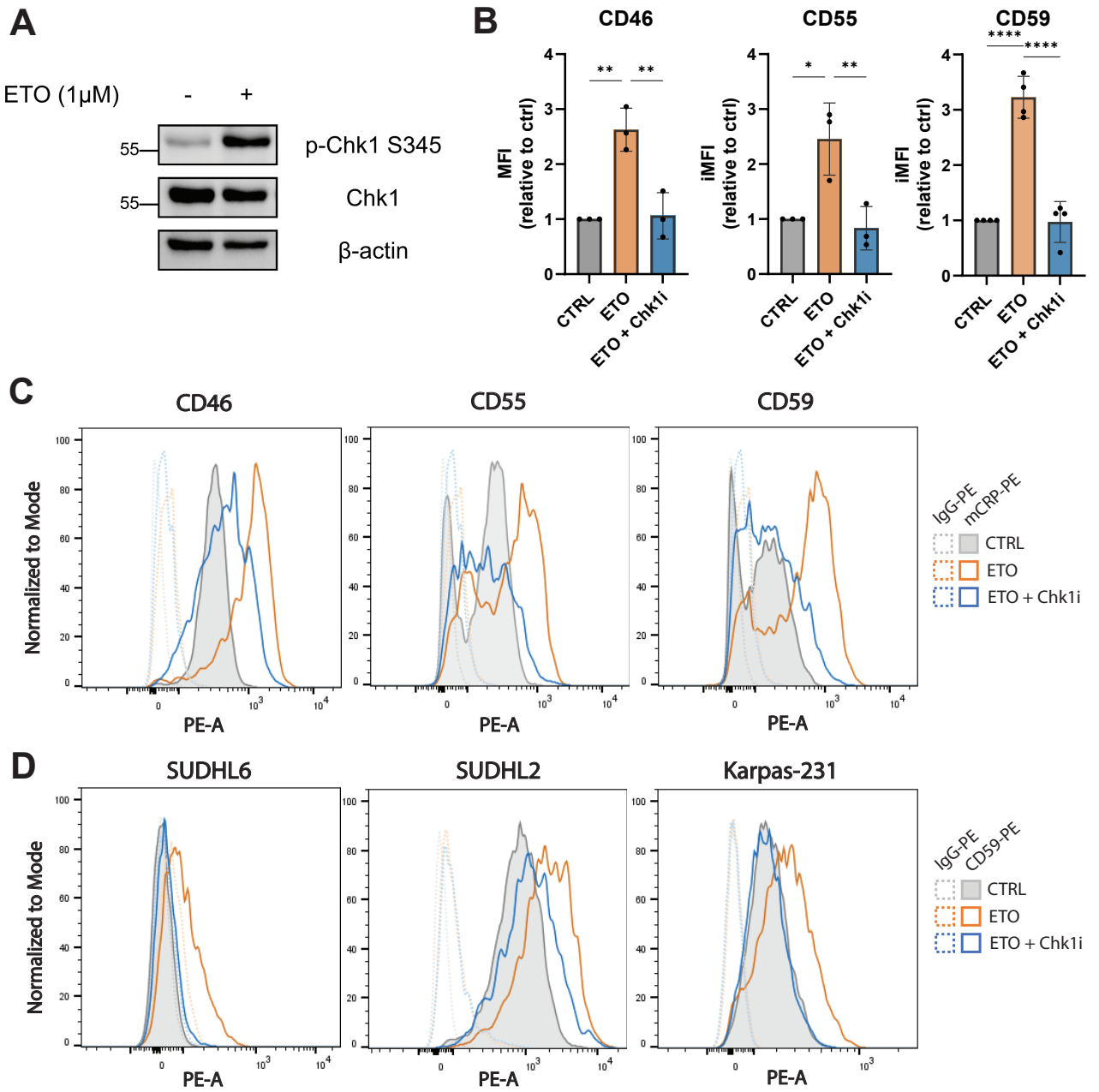
A
ETO (1μM)
-
+
55
55
p-Chk1 S345
Chk1
β-actin
B
CD46
CD55
CD59
MFI (relative to ctrl)
iMFI (relative to ctrl)
CTRL
ETO
ETO + Chk1i
C
CD46
CD55
CD59
Normalized to Mode
PE-A
IgG-PE
mCRP-PE
CTRL
ETO
ETO + Chk1i
D
SUDHL6
SUDHL2
Karpas-231
Normalized to Mode
PE-A
IgG-PE
CD59-PE
CTRL
ETO
ETO + Chk1i

Figure 5

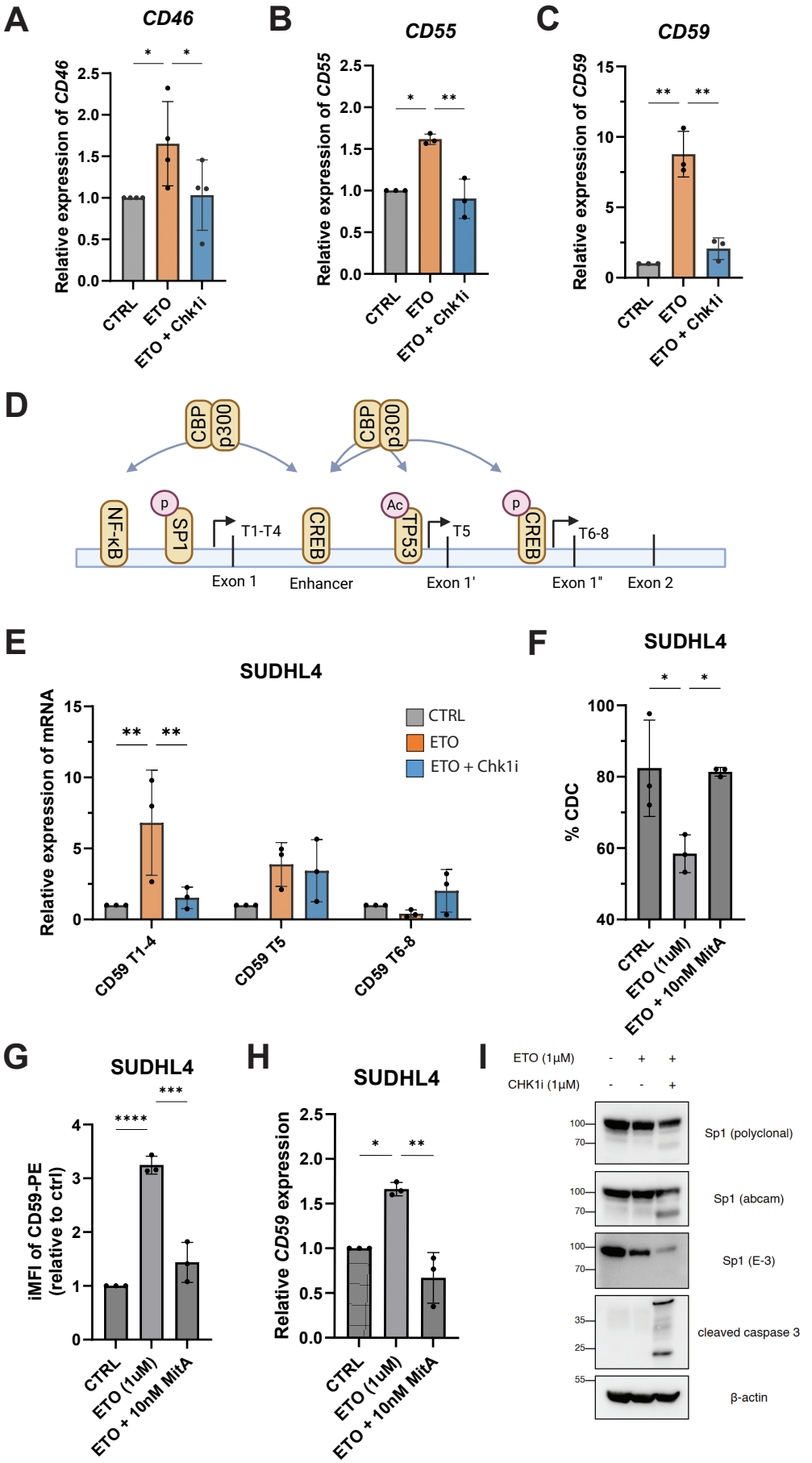
A
CD46
Relative expression of CD46
CTRL
ETO
ETO + Chk1i
B
CD55
Relative expression of CD55
C
CD59
Relative expression of CD59
D
CBP
p300
NF-kB
SP1
CREB
TP53
T1-T4
T5
T6-8
Exon 1
Enhancer
Exon 1'
Exon 1"
Exon 2
E
SUDHL4
Relative expression of mRNA
CTRL
ETO
ETO + Chk1i
CD59 T1-4
CD59 T5
CD59 T6-8
F
SUDHL4
% CDC
ETO (1uM)
ETO + 10nM MitA
G
SUDHL4
iMFI of CD59-PE (relative to ctrl)
H
SUDHL4
Relative CD59 expression
I
ETO (1μM)
CHK1i (1μM)
Sp1 (polyclonal)
Sp1 (abcam)
Sp1 (E-3)
cleaved caspase 3
β-actin

Figure 6

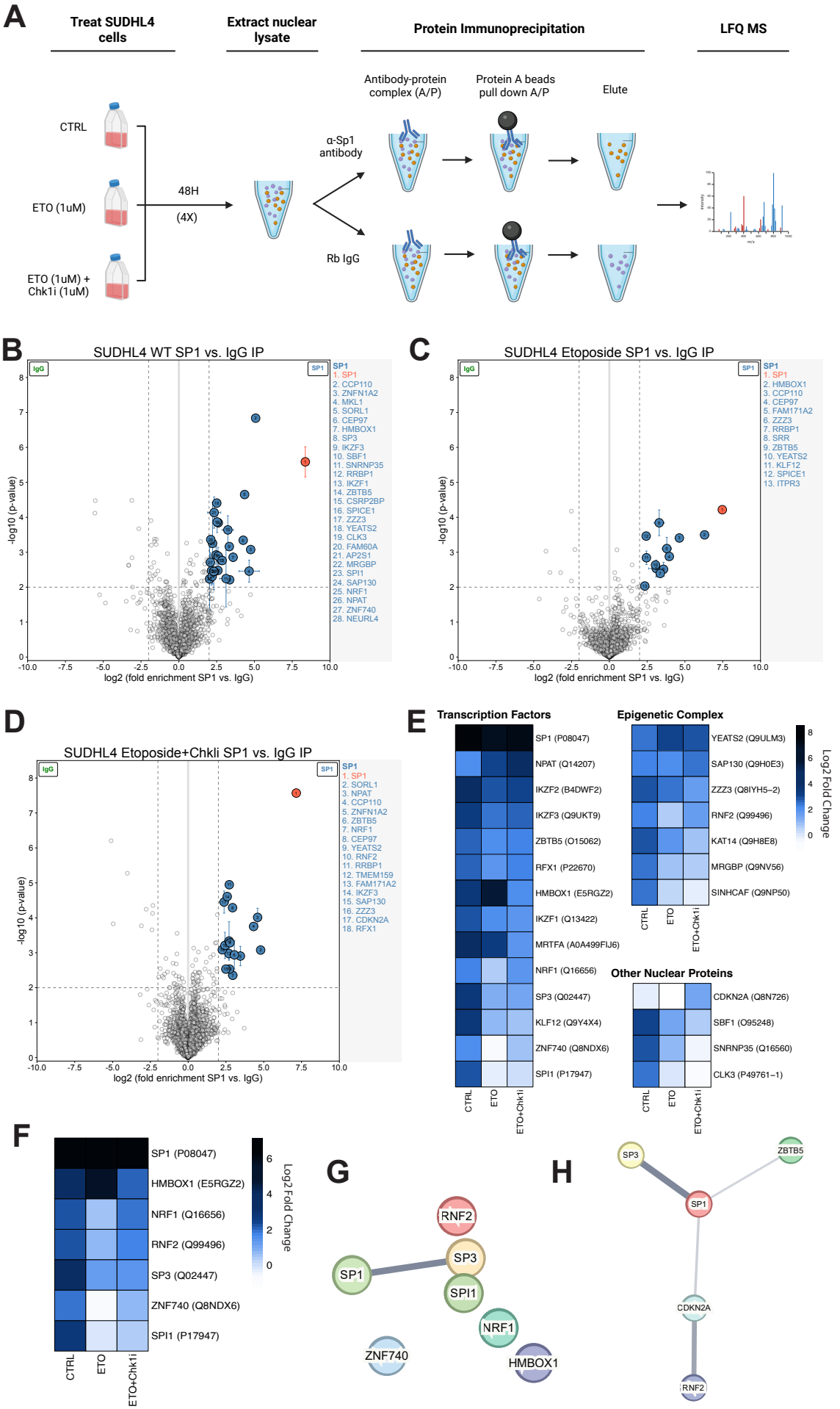
A
Treat SUDHL4 cells
Extract nuclear lysate
Protein Immunoprecipitation
LFQ MS
CTRL
ETO (1uM)
ETO (1uM) + Chk1i (1uM)
48H
(4X)
α-Sp1 antibody
Rb IgG
Antibody-protein complex (A/P)
Protein A beads pull down A/P
Elute
B
SUDHL4 WT SP1 vs. IgG IP
IgG
SP1
SP1
1. SP1
2. CCP110
3. ZNFN1A2
4. MKL1
5. SORL1
6. CEP97
7. HMBOX1
8. SP3
9. IKZF3
10. SBF1
11. SNRNP35
12. RRBP1
13. IKZF1
14. ZBTB5
15. CSRP2BP
16. SPICE1
17. ZZZ3
18. YEATS2
19. CLK3
20. FAM60A
21. AP2S1
22. MRGBP
23. SPI1
24. SAP130
25. NRF1
26. NPAT
27. ZNF740
28. NEURL4
-log10 (p-value)
log2 (fold enrichment SP1 vs. IgG)
C
SUDHL4 Etoposide SP1 vs. IgG IP
IgG
SP1
SP1
1. SP1
2. HMBOX1
3. CCP110
4. CEP97
5. FAM171A2
6. ZZZ3
7. RRBP1
8. SRR
9. ZBTB5
10. YEATS2
11. KLF12
12. SPICE1
13. ITPR3
-log10 (p-value)
log2 (fold enrichment SP1 vs. IgG)
D
SUDHL4 Etoposide+Chkli SP1 vs. IgG IP
IgG
SP1
SP1
1. SP1
2. SORL1
3. NPAT
4. CCP110
5. ZNFN1A2
6. ZBTB5
7. NRF1
8. CEP97
9. YEATS2
10. RNF2
11. RRBP1
12. TMEM159
13. FAM171A2
14. IKZF3
15. SAP130
16. ZZZ3
17. CDKN2A
18. RFX1
-log10 (p-value)
log2 (fold enrichment SP1 vs. IgG)
E
Transcription Factors
SP1 (P08047)
NPAT (Q14207)
IKZF2 (B4DWF2)
IKZF3 (Q9UKT9)
ZBTB5 (O15062)
RFX1 (P22670)
HMBOX1 (E5RGZ2)
IKZF1 (Q13422)
MRTFA (A0A499FIJ6)
NRF1 (Q16656)
SP3 (Q02447)
KLF12 (Q9Y4X4)
ZNF740 (Q8NDX6)
SPI1 (P17947)
CTRL
ETO
ETO+Chk1i
Epigenetic Complex
YEATS2 (Q9ULM3)
SAP130 (Q9H0E3)
ZZZ3 (Q8IYH5–2)
RNF2 (Q99496)
KAT14 (Q9H8E8)
MRGBP (Q9NV56)
SINHCAF (Q9NP50)
CTRL
ETO
ETO+Chk1i
Log2 Fold Change
Other Nuclear Proteins
CDKN2A (Q8N726)
SBF1 (O95248)
SNRNP35 (Q16560)
CLK3 (P49761–1)
CTRL
ETO
ETO+Chk1i
F
SP1 (P08047)
HMBOX1 (E5RGZ2)
NRF1 (Q16656)
RNF2 (Q99496)
SP3 (Q02447)
ZNF740 (Q8NDX6)
SPI1 (P17947)
CTRL
ETO
ETO+Chk1i
Log2 Fold Change
G
RNF2
SP3
SP1
SPI1
NRF1
ZNF740
HMBOX1
H
SP3
ZBTB5
SP1
CDKN2A
RNF2

Figure 7

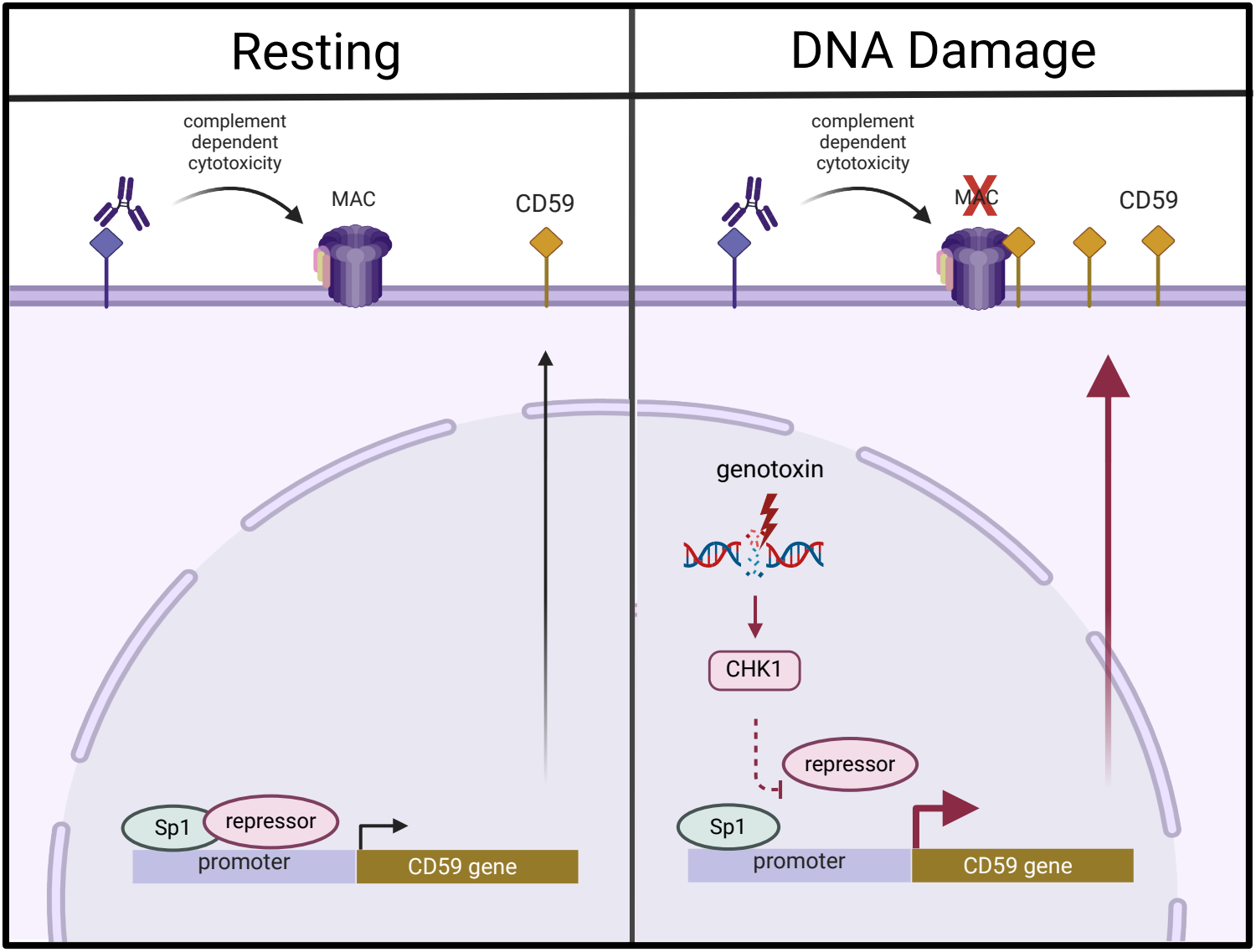
Resting
DNA Damage
complement dependent cytotoxicity
MAC
CD59
complement dependent cytotoxicity
MAC
CD59
genotoxin
CHK1
repressor
Sp1
repressor
promoter
CD59 gene
Sp1
promoter
CD59 gene